Journal of Alloys and Compounds 509 (2011) 414–420

Contents lists available at ScienceDirect

Journal of Alloys and Compounds

journal homepage: www.elsevier.com/locate/jallcom

Structural, morphological and electrical properties of spray deposited nano-crystalline CeO_2 thin films

B.B. Patil[a,*], S.H. Pawar[b]

[a] Department of Chemical Engineering, I.I.T. Delhi, New Delhi 110016, India
[b] D.Y. Patil University, Kasaba Bawada, Kolhapur 416 006, (M.S), India

ARTICLE INFO

Article history:
Received 7 June 2010
Received in revised form 5 September 2010
Accepted 8 September 2010
Available online 17 September 2010

Keywords:
Fuel cells
Oxide materials
Chemical synthesis
Crystal structure
Atomic force microscopy (AFM)

ABSTRACT

Nanocrystalline, uniform, dense, and adherent cerium oxide (CeO_2) thin films have been successfully deposited by a simple and cost effective spray pyrolysis technique. CeO_2 films were deposited at low substrate and annealing temperatures of 350 °C and 500 °C, respectively. Films were characterized by differential thermal analysis, X-ray diffraction, scanning electron microscopy, atomic force microscopy; two probe resistivity method and impedance spectroscopy. X-ray diffraction analysis revealed the formation of single phase, well crystalline thin films with cubic fluorite structure. Crystallite size was found to be in the range of 10–15 nm. AFM showed formation of smooth films with morphological grain size 27 nm. Films were found to be highly resistive with room temperature resistivity of the order of 10^7 Ω cm. Activation energy was calculated and found to be 0.78 eV. The deposited film showed high oxygen ion conductivity of 5.94×10^{-3} S cm^{-1} at 350 °C. Thus, the deposited material shows a potential application in intermediate temperature solid oxide fuel cells (IT-SOFC) and might be useful for μ-SOFC and industrial catalyst applications.

1. Introduction

Ceria (CeO_2), a stable fluorite-type oxide, is an attractive material with multiple applications such as protective coating on superconducting thin films [1], corrosion resistance coatings [2], electrochromic layers [3], gate insulators on silicon [4], the key component in the three way catalyst [5], in microelectronics, optoelectronics and photo catalysis [6].

Recently, ceria based thin films have shown various applications in the field of solid oxide fuel cells (SOFC) too. Ceria-based thin films can be used as solid electrolytes in SOFC due to their higher ionic conductivity with respect to stabilized zirconia and a lower cost in comparison with lanthanum gallate based phases [7,8]. Ceria has catalytic activity for the oxidation of hydrocarbon fuels hence is included in the anode to enhance anode performance [9,10]. Doped or undoped ceria oxides are commonly applied as sulfur tolerant component in metal cermet anodes due to good performance at lower cost relative to available alternatives. CeO_2 has been widely used in sulfur removal processes and adds coking resistance in catalytic processes. When used together with Ni to form a cermet anode CeO_2 also clearly suppresses the sulfur poisoning of Ni, which indicates that CeO_2 efficiently acts as a H_2S absorbent in fuel cells [11,12]. Due to mixed ionic conductivity, reduced ceria also increases the length of the three phase boundary [13].

There are different methods to synthesize the CeO_2 thin films such as, sputtering [14], laser ablation [15], chemical vapor deposition [16], sol–gel deposition [17], microwave induced combustion [18], anodic electrodeposition [19], spray pyrolysis [20–26].

Spray pyrolysis is an integrated process, which consists of three consecutive steps, namely atomization of liquid into droplets, traveling of droplets with atomization gas and deposition of droplets on to three-dimensional reform. Unlike many other film deposition techniques, spray pyrolysis technique offers an attractive way for the formation of thin films [27].

In the present investigation, nano-crystalline, uniform, dense, and adherent cerium oxide thin films have been successfully deposited by a simple and cost effective spray pyrolysis technique at low substrate and annealing temperature of 350 °C and 500 °C, respectively. Deposited films have high oxygen ion conductivity than reported by others. The films were characterized for their structural, morphological and transport properties and the results are reported in the paper.

2. Experimental

Ceria films were synthesized using spray pyrolysis technique by dissolving cerium nitrate $Ce(NO_3)_3{\cdot}6H_2O$ (99.9% pure, Loba chemicals) in double distilled water. Spray system used is described in detail elsewhere [28]. Ultrasonically cleaned plane glass plates (3.7 cm × 1.2 cm) were used as substrates. Use of double distilled water as solvent and glass plates as substrates are among the parame-

* Corresponding author. Tel.: +91 11 2659 1035; fax: +91 11 2685 1169.
E-mail address: bhartibpatil_2003@yahoo.co.in (B.B. Patil).

0925-8388/$ – see front matter © 2010 Elsevier B.V. All rights reserved.
doi:10.1016/j.jallcom.2010.09.045

ters that has made the film formation process cost effective. Optimized preparative parameters for the deposition of thin films of ceria material were, spray rate – 5 ml/min, concentration of precursor solution – 0.1 M, quantity – 40 ml. Substrate temperature was varied from 300 to 400 °C with an interval of 50 °C and these films were described as F_{300}, F_{350} and F_{400}.

Deposited films were allowed to cool slowly. These films were further annealed in tube furnace at 500 °C for 2 h and described as F_{A300}, F_{A350} and F_{A400}. These films were then characterized by X-ray diffraction (XRD) technique. From XRD studies, optimized substrate temperature for the deposition of CeO_2 films was found to be 350 °C. In order to see effect of annealing temperature on phase formation, film deposited at 350 °C substrate temperatures was then annealed in tube furnace at various temperatures such as 400 °C, 450 °C and 500 °C. These films were described as F_{H400}, F_{H450} and F_{H500}, respectively. Here film $F_{A350} = F_{H500}$. Description of the samples is given in Table 1. Film thickness was calculated by using weight difference method [29]:

$$t = \frac{\text{weight difference}}{A\rho} \quad (1)$$

where A is the area of the film and ρ is the density of the bulk material and for ceria density was taken as 7.215 g/cm^3. Film thickness was found to be 0.91 μm.

The material from as deposited thin films was scratched out from the substrate and then differential thermal analysis (DTA) and thermogravimetric analysis (TGA) were studied by using an instrument SDT-2960, TA Inc., USA, with a heating rate 10 °C/min from 10 to 1000 °C in air environment. The films were characterized by XRD technique using Phillips PW-1710 diffractometer with CuK_α radiation having wavelength 1.5424 Å. The spectra were obtained over the 2θ range 10–100°. The diffractometer was operated at 40 kV and 30 mA. The crystallite size was determined by using Scherrer's formula.

Two-probe resistivity method was used to study the effect of substrate temperature on the electrical property of CeO_2 film in the temperature range 27–425 °C. The method was reported in detail in our previous work [27]. Scanning electron microscope (SEM) image of the film was taken by using SEM model, JEOL JSM 6360. Grain size and surface roughness of the film was measured by using atomic force microscope (AFM) model, nanoscope E of Digital Instruments, USA in contact mode, with V-shape silicon nitride cantilever of length 100 μm and spring constant 0.58 N/m. Two-probe impedance measurement technique was used for impedance measurement. Impedance measurement of the film was carried out in air at 350 °C using LCR meter bridge (model HP 4284A) with frequency range of 100 Hz to 1 MHz and amplitude of 1 V. In this technique a brass block was used as a sample holder cum heater. The area of the film on the glass substrate was defined as 1.2 cm × 1.2 cm and silver paste was applied to ensure the ohmic contact to the film. Two press contacts were made to the film with the help of pointed brass screws. Cromel–Alumel thermocouple was used to measure the temperature.

3. Results and discussion

3.1. DTA–TGA study

DTA–TGA studies were carried out in order to find the post heat treatment temperature for the CeO_2 phase formation. CeO_2 films were deposited at 350 °C substrate temperature on glass substrate and powder was scratched from the substrate for the study. Fig. 1 shows the DTA–TGA curve of the spray deposited ceria powder. DTA study shows flattened exothermic peak at 279 °C, the peak is due to removal of the remains of nitrate precursor solution present in the powder. TGA curve shows weight loss of 2.8% up to 350 °C above this temperature not much loss in weight was observed. Thus, DTA–TGA studies revealed that, the decomposition temperature for the CeO_2 phase formation is in the range of 300–350 °C. The following reaction proceeds during spray pyrolysis:

$$Ce(NO_3)_3 \cdot 6H_2O + H_2O \overset{300-350\,^\circ C}{\longrightarrow} CeO_{2(s)} + 7H_2O_{(g)} + 3NO_2 + (1/2)O_2 \quad (2)$$

Hence, in order to remove the remains of the precursor solution present in as deposited films, there was necessity to further post heat these films. From Fig. 1, it is clear that the material is completely decomposed after 350 °C. The substrates used were of glass and glass starts melting above 500–550 °C [27]. Therefore, in the present investigation, films were post heat treated at 500 °C for 2 h in tube furnace.

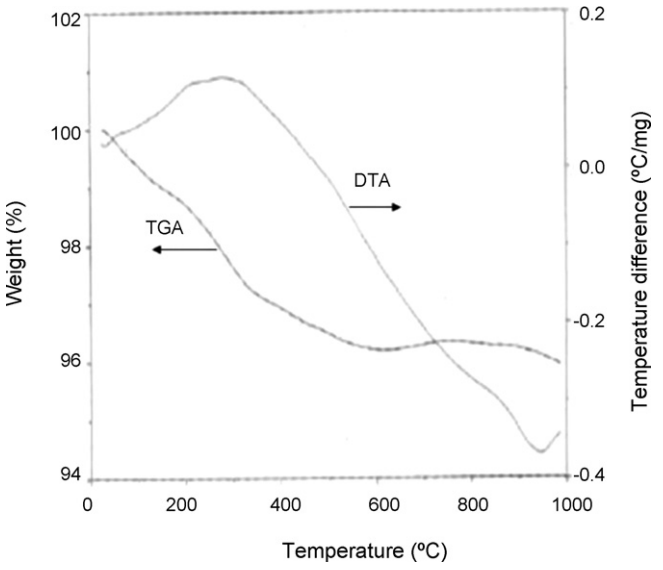

Fig. 1. The simultaneous DTA–TGA curves of spray deposited CeO_2 powder.

3.2. Effect of Substrate Temperature on the XRD patterns of the ceria films

In spray pyrolysis technique, substrate temperature plays an important role in film formation. In order to study the effect of substrate temperature on the CeO_2 phase formation, F_{A300}, F_{A350}, F_{A400}, and F_{350} films were characterized by using X-ray diffractometer. Fig. 2 shows the XRD patterns of these CeO_2 films. It has been reported earlier that when thin films are deposited by spray pyrolysis the material is amorphous and crystallization occurs during the first annealing for temperatures above the film deposition temperature [26,30]. But from Fig. 2, it is clear that not only annealed films but also as deposited films were polycrystalline in nature. All peaks have been identified and indexed from the known patterns of the standard data files [31].

Average lattice constant 'a' of F_{A300}, F_{A350} and F_{A400} and F_{350} CeO_2 films have been calculated and were found to be 5.4116 Å, 5.4088 Å, 5.4176 Å and 5.4199 Å, respectively. The 'a' values for all samples matches well with the reported values [20,32,33].

The observed and standard 'd' values of the spray deposited CeO_2 thin films are listed in Table 2. It is observed that for all films (1 1 1) reflection is most prominent, also number of peaks corresponding to the ceria phase found to increase with increase in substrate temperature. No peak corresponding to elemental cerium deposition was observed, confirming the formation of single phase ceria films. The comparison of (1 1 1) peak intensity with substrate temperature shows that the peak intensity of (1 1 1) peak is less for F_{A300}, F_{A400} films than for F_{A350}. It means that well crystalline film of CeO_2 is forming at 350 °C substrate temperature, and hence this substrate temperature was optimized for further study.

The highest intensity X-ray diffraction (1 1 1) peak lying at about $2\theta = 28°$ has been further analyzed to yield the crystallite size of the ceria material by using the Scherrer's formula [34]:

$$d = \frac{0.9\lambda}{\beta \cos\theta} \quad (3)$$

where d is the crystallite size of the material, λ is the wavelength of the X-ray radiation, β is the full width at half maxima and θ is the angle of diffraction.

Crystallite size of F_{A300}, F_{A350} and F_{A400} and F_{350} ceria films were found to be 13, 15, 11 and 10 nm, respectively. Not much difference in crystallite size with substrate temperature was observed. The synthesis of ultra fine ceria material is of practical importance

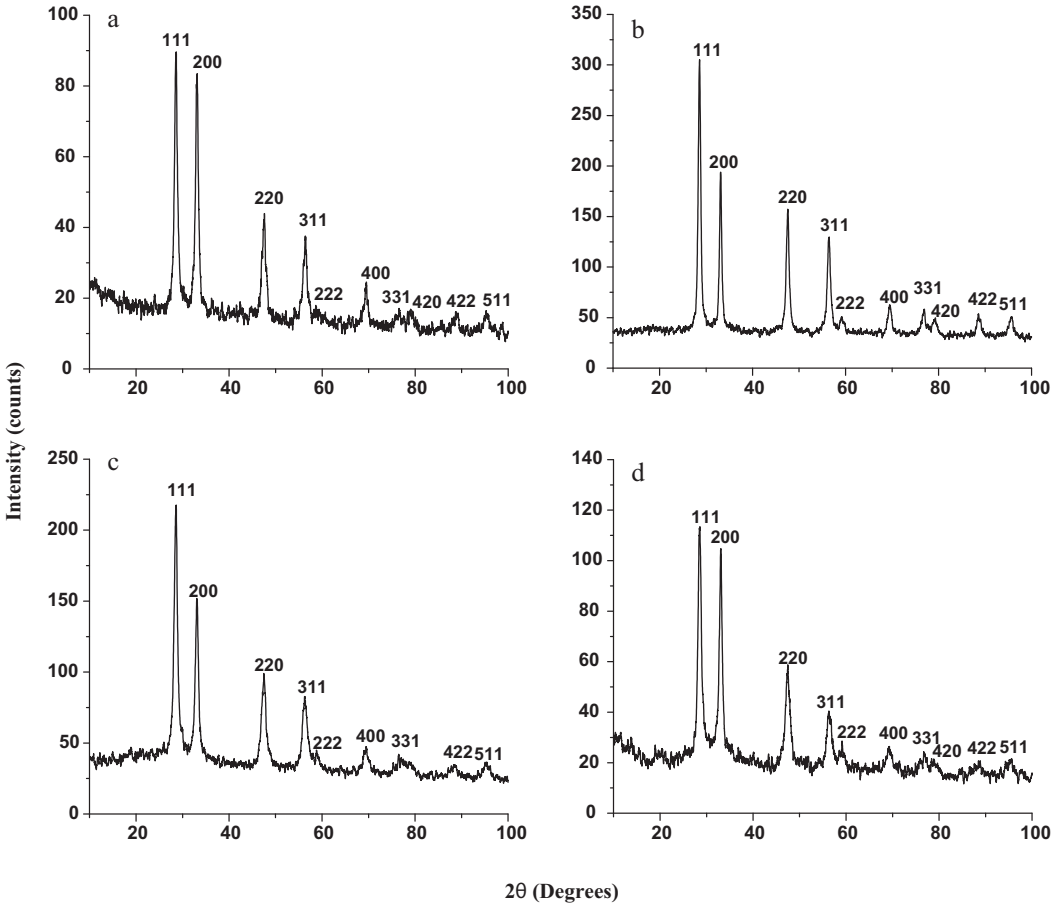

Fig. 2. The XRD patterns of (a) F_{A300}, (b) F_{A350}, (c) F_{A400}, and (d) F_{350} CeO_2 films.

to get dense sintered product at a lower sintering temperature, in particular when problem of change of valence state of cerium (Ce^{4+} to Ce^{3+}) is associated during sintering at higher temperature (>1300 °C) [35]. Hence nanocrystalline cerium oxide deposited by spray pyrolysis technique can help to reduce the sintering temperature.

3.3. Effect of annealing temperature on the XRD patterns of the ceria films

Fig. 3 shows XRD patterns of CeO_2 films deposited at 350 °C substrate temperatures and annealed at 400 °C – F_{H400}, 450 °C – F_{H450} and 500 °C – F_{H500} for 2 h. Deposited ceria films are found to be polycrystalline in nature.

Lattice constants '*a*' of F_{H400}, F_{H450} and F_{H500}, F_{350} have been calculated and found to be 5.4091 Å, 5.4141 Å, 5.4089 Å, and 5.4199 Å, respectively. The '*a*' values for all samples matches well with the reported values for cubic fluorite CeO_2 phases [20,32,33].

The *d* values and the lattice constants of different planes for the films are listed in Table 3. It is observed that, the number of peaks corresponding to ceria phase increase with increase in the annealing temperature. This might be due to the increase in the crystalline nature of the film with annealing temperature [26].

The intensity of (1 1 1) plane is strongest for all the films. Also for all films no phase corresponding to cerium has been observed confirming the direct formation of ceria phase.

Crystallite size of ceria films were calculated by using Scherrer's formula and were found to be 10, 14, 11, 15 nm, respectively. Comparison between the XRD patterns of F_{350}, F_{A350} showed that, as deposited CeO_2 film was less crystalline than that of film annealed at 500 °C for 2 h. From Tables 2 and 3 it has been observed that all major reflections for CeO_2 cubic phase were observed for F_{A350}. Thus, optimized substrate and annealing temperature for deposition of nano-crystalline, adherent, single phase cubic CeO_2 thin film were found to be 350 °C and 500 °C, respectively.

3.4. Morphological studies

3.4.1. SEM studies

Surface morphology of ceria film deposited at 350 °C substrate temperature and post heat treated at 500 °C (F_{A350}) is shown in Fig. 4. The SEM image shows the formation of CeO_2 film with

Table 1
Description of the samples.

F_{350}	As deposited CeO_2 film at 350 °C substrate temperature
F_{A300}	CeO_2 film deposited at 300 °C substrate temperature and post heat treated at 500 °C
F_{A350}	CeO_2 film deposited at 350 °C substrate temperature and post heat treated at 500 °C
F_{A400}	CeO_2 film deposited at 400 °C substrate temperature and post heat treated at 500 °C
F_{H400}	CeO_2 film deposited at 350 °C substrate temperature and post heat treated at 400 °C
F_{H450}	CeO_2 film deposited at 350 °C substrate temperature and post heat treated at 450 °C
	Here $F_{A350} = F_{H500}$.

Table 2
Comparison of *d* values and lattice constants of F_{A300}, F_{A350}, F_{A400}, F_{350} CeO_2 films.

h k l	Std. *d* (Å)	F_{A300} (Å)		F_{A350} (Å)		F_{A400} (Å)		F_{350} (Å)	
		d_{obs}	a_{obs}	d_{obs}	a_{obs}	d_{obs}	a_{obs}	d_{obs}	a_{obs}
111	3.1234	3.1240	5.4110	3.1241	5.4110	3.1171	5.3989	3.1413	5.4408
200	2.7056	2.6968	5.3937	2.7067	5.4135	2.7079	5.4158	2.7119	5.4238
220	1.9134	1.9117	5.4072	1.9113	5.4061	1.9142	5.4141	1.9150	5.4162
311	1.6318	1.6348	5.4220	1.6320	5.4128	1.6358	5.4253	1.6318	5.4288
222	1.5622	–	–	1.5634	5.4159	–	–	1.5603	5.4052
400	1.3531	1.3548	5.4192	1.3533	5.4132	1.3550	5.4200	–	–
331	1.2415	–	–	1.2402	5.4061	1.2461	5.4318	1.2400	5.4050
420	1.2101	–	–	1.2063	5.3947	–	–	–	–
422	1.1048	1.1037	5.4070	1.1037	5.4068	–	–	–	–
511	1.0415	1.0434	5.4216	1.0410	5.4089	–	–	–	–

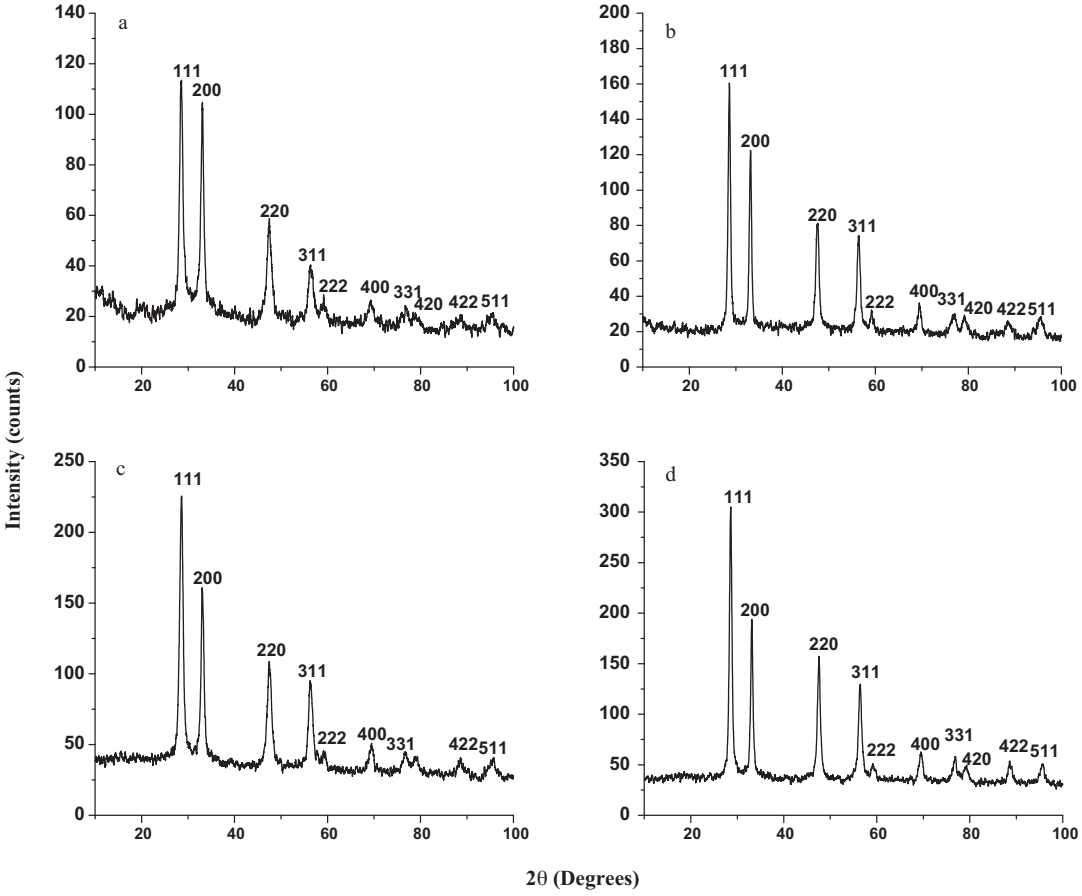

Fig. 3. The XRD patterns of (a) F_{350}, (b) F_{H400}, (c) F_{H450}, and (d) F_{H500} CeO_2 films.

Table 3
Comparison of d values and lattice constants of F_{350}, F_{H400}, F_{H450}, F_{H500} CeO_2 films.

h k l	Std. *d* (Å)	F_{350} (Å)		F_{H400} (Å)		F_{H450} (Å)		F_{H500} (Å)	
		d_{obs}	a_{obs}	d_{obs}	a_{obs}	d_{obs}	a_{obs}	d_{obs}	a_{obs}
111	3.1234	3.1413	5.4409	3.1182	5.4080	3.1214	5.4063	3.1241	5.4110
200	2.7056	2.7119	5.4238	2.7068	5.4135	2.7135	5.4269	2.7068	5.4135
220	1.9134	1.9150	5.4162	1.9076	5.3954	1.9172	5.4226	1.9114	5.4061
311	1.6318	1.6318	5.4288	1.6326	5.4147	1.6340	5.4191	1.6321	5.4128
222	1.5622	1.5604	5.4052	1.5631	5.4146	1.5576	5.3955	1.5634	5.4159
400	1.3531	–	–	1.3532	5.4128	1.3541	5.4160	1.3533	5.4132
331	1.2415	1.2400	5.4050	1.2407	5.4079	1.2424	5.4153	1.2403	5.4061
420	1.2101	–	–	1.2090	5.4068	–	–	1.2063	5.3947
422	1.1048	–	–	–	–	1.1055	5.4155	1.1037	5.4068
511	1.0415	–	–	1.0423	5.4159	1.0412	5.4102	1.0410	5.4089

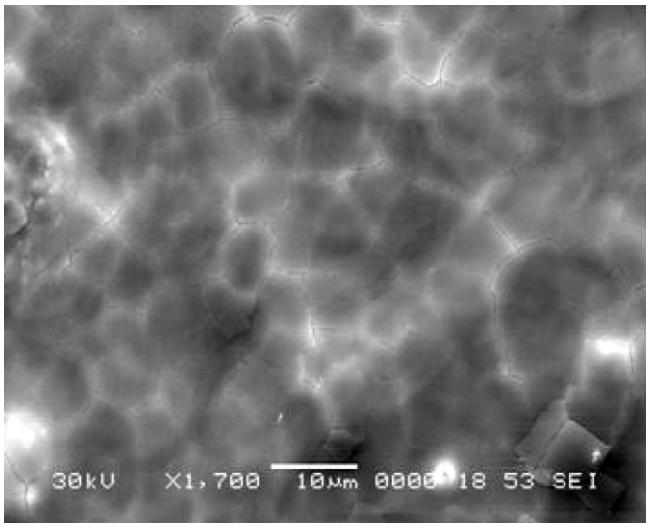

Fig. 4. SEM image of F_{A350} CeO_2 film.

smooth surface. Also, extensive cracking of the film can be seen. This is probably due to shrinkage of the film upon drying. Such type of cracking of CeO_2 film has also been observed for electrophoresis [36], anodic electrodeposition [19] and CeO_2 films deposited on mica flakes [37]. Another reason for cracks might be high concentration of precursor solution, 0.1 M.

In spray pyrolysis technique average crystallite size depends on both the deposition temperature and the concentration of precursor solution. Many researchers who have used the spray pyrolysis process for preparing thin films reported that, as concentration increases the peak intensity increases and peak become narrower indicating a better crystallinity. This improvement in crystallinity with concentration can be attributed to the increase of the film thickness [38,39]. So in the present work high concentration was tried.

But because of high concentration some cracks due to internal stress were observed. Such type of cracking was reported earlier in spray deposited CeO_2 films [39].

3.4.2. AFM studies

The ability of atomic force microscope (AFM) to create three-dimensional micrographs with resolution down to the nanometer to the angstrom scales has made it essential tool for imaging surfaces. AFM was used to determine grain size and the surface roughness of the film. Fig. 5 shows two-dimensional and three-dimensional AFM images of F_{A350} CeO_2 film, respectively. Fig. 5(a) shows that the film is made up of small granules having nearly spherical shape. Surface roughness of the film was calculated with a statistical parameter-root mean square (rms or R_q).

$$R_q = \sqrt{\frac{\sum_{i=1}^{N}\left(Z_i - Z_{avg}\right)^2}{N}} \quad (4)$$

where Z_{avg} is the average of Z values within given area, Z_i is the current and N is the number of points within given area. From Fig. 5(a), calculated grain size and surface roughness were found to be 27 nm and 1.6 nm, respectively, showing formation of smooth CeO_2 film. The grain size was found to be less than that of reported earlier [24].

3.5. DC electrical resistivity study

Two-probe resistivity method was used to study the electrical properties of CeO_2 films deposited at different substrate temperatures and heat treated at 500 °C. The resistivity of the film was

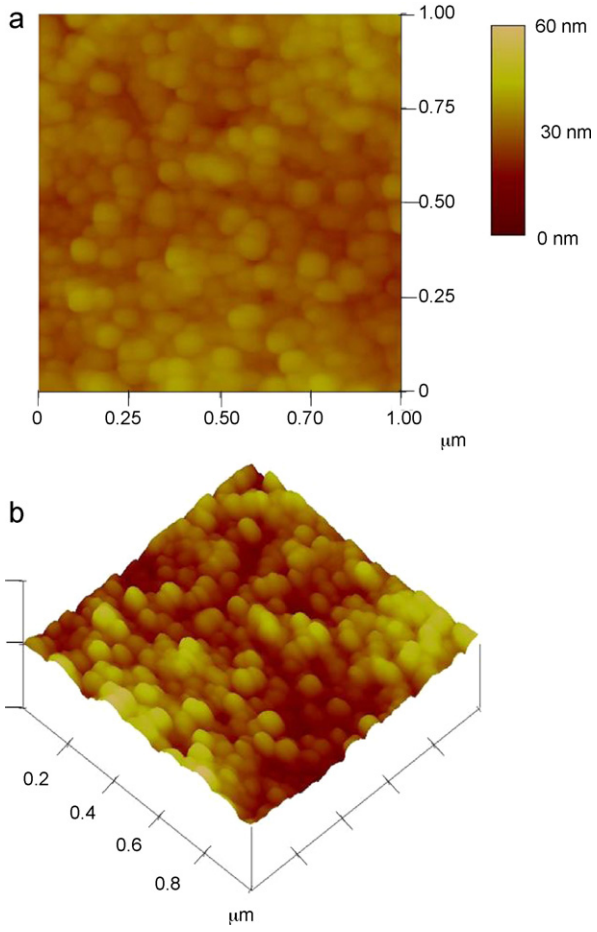

Fig. 5. AFM images of F_{A350} CeO_2 thin film: (a) two-dimensional and (b) three-dimensional.

studied in the temperature range 27–425 °C. Measurements were carried out under air atmosphere.

The plot of log ρ vs $1/T$ for F_{A300}, F_{A350}, and F_{A400} is shown in Fig. 6. It is observed that, the resistivity of all the films decreases with increase in the temperature showing semiconducting nature. The room temperature resistivities of F_{A300}, F_{A350}, and F_{A400} films are of the order of 10^7 Ω cm.

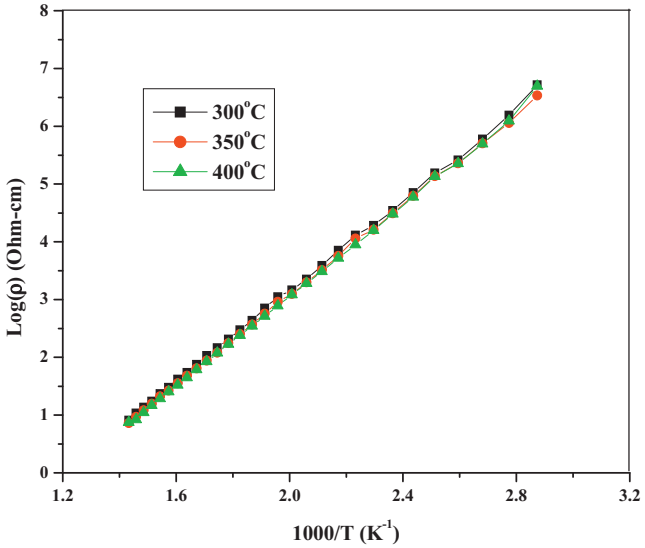

Fig. 6. Plot of log ρ vs. $1/T$ for F_{A300}, F_{A350}, and F_{A400} CeO_2 films.

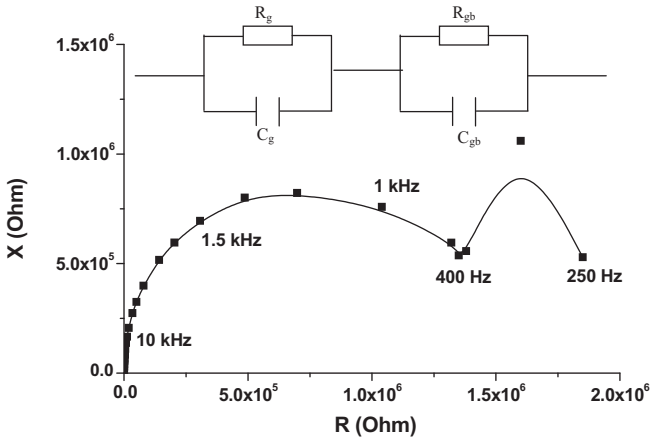

Fig. 7. Nyquist plot of F_{A350} CeO_2 film at 350 °C.

Activation energies of the deposited films were calculated by using the relation [40]:

$$\rho = \rho_0 \exp\left(\frac{E_a}{kT}\right) \quad (5)$$

where ρ is the resistivity, E_a is the activation energy, k is the Boltzmann constant and T is the absolute temperature. Activation energy values for F_{A300}, F_{A350}, and F_{A400} films were found to be 0.78, 0.78 and 0.79 eV, respectively, which are similar to the value of 0.78 eV for the activation energy of doped ceria [27,41,42] and less than that of undoped ceria, 1.03 eV [43].

3.6. Complex impedance measurements

The method of complex impedance analysis [44] has emerged as very powerful tool for separating out the contributions due to intra-grain, grain boundary and electrode processes. Fig. 7 shows complex impedance plot of resistance (R) vs reactance (X) for F_{A350} CeO_2 film measured at 350 °C. The frequency was varied from 100 Hz to 1 MHz. From the figure it is seen that, the impedance plot was divided into two semicircles on the X-axis. The semicircle in the higher frequency and lower frequency range may correspond to oxygen ion migration in the bulk and across the grain boundaries, respectively [45]. It is modeled as an equivalent circuit comprising of combination of bulk (R_g) and grain boundary (R_{gb}) resistance and bulk (C_g) and grain boundary (C_{gb}) capacitance as shown inset of Fig. 7. Similar nature of impedance plot was reported earlier in case of doped ceria [46,47] and undoped ceria [48].

From Fig. 7, the bulk resistance of the material at 350 °C was found to be 1.85×10^6 Ω. A.C. conductivity of the film was calculated by using equation

$$\sigma_{ac} = \frac{d}{RA} \quad (6)$$

where σ_{ac} is the conductivity S cm^{-1}, R is the resistance measured (Ω), d is the distance between voltage electrodes (cm) and A is the cross sectional area of the electrode (cm^2). A.C. conductivity is found to be high as 5.94×10^{-3} S cm^{-1} at 350 °C than that reported for the bulk 1.2×10^{-6} S cm^{-1} at 600 °C [49].

It has been reported that a microcrystalline material fares far better in terms of ionic conductivity than that the nanocrystalline material [50]. It is also reported that, the grain boundary resistivity changes with the grain size. When the grain size decreases from a few micrometers to the nano-level, the grain boundaries show unusually high conductivity [51–53]. This is due to the fact that in nano-crystalline materials grain boundaries have high defect densities and the atoms there have high mobility. These are the two important factors for increase in the ionic conductivity. Hence, the ionic conductivity may be significantly enhanced in nanocrystalline materials compared to the microcrystalline ones [51], same has been observed in the present work.

4. Conclusions

Nano-crystalline, uniform, dense and adherent cerium oxide thin films have been deposited successfully by a simple and cost effective spray pyrolysis technique at low substrate and annealing temperature of 350 °C and 500 °C, respectively. All films were found to be single phase and well crystalline with most prominent (1 1 1) reflection. Crystallinity of the film was found to increase with increase in substrate and annealing temperature. Crystallite size was found to be in the range of 10–15 nm. AFM showed formation of smooth films with morphological grain size 27 nm. The deposited film showed high oxygen ion conductivity, 5.94×10^{-3} S cm^{-1} at 350 °C. Due to its nano-crystalline nature, the deposited ceria material will have high sinterability, high surface area and hence can have various applications such as in intermediate temperature solid oxide fuel cell, gas sensors, electrochromic smart window devices, in corrosion protection and catalysis.

Acknowledgements

One of the authors B.B.P. is thankful to the Ministry of New and Renewable Energy (MNRE), New Delhi for providing financial assistance. They are also indebted to U.G.C., Delhi for financial support. The co-operation rendered by Ms. Siddhi and Mr. Rahul during the manuscript preparation has been greatly acknowledged.

References

[1] R. Aguiar, F. Sancher, C. Ferrater, M. Varela, Thin Solid Films 306 (1997) 74.
[2] R. Di Maggio, S. Rosi, L. Fedrizzi, P. Scardi, Surf. Coat. Technol. 89 (1997) 292.
[3] R.D. Monte, J. Kasper, J. Mater. Chem. 15 (2005) 663.
[4] L. Tye, N.A. El-Masry, T. Chikyow, P. Mc Larty, S.M. Bedair, Appl. Phys. Lett. 65 (1994) 3081.
[5] Trovarelli, Catal. Rev. Sci. Eng. 38 (4) (1996) 439.
[6] Y. Jiang, N. Bahlawane, J. Alloys Compd. 485 (2009) L52.
[7] E. Jud, L.J. Gauckler, J. Electroceram. 15 (2005) 159.
[8] S.J. Skinner, J.A. Kilner, Mater. Today 6 (2003) 30.
[9] S. McIntosh, J.M. Vohs, R.J. Gorte, Electrochim. Acta 47 (2000) 3815.
[10] S.Z. hao, R.J. Gorte, Appl. Catal. A 248 (2003) 9.
[11] M.F. Stephanopoulos, M. Sakbodin, Z. Wang, Science 312 (2006) 1508.
[12] H. Devianto, J. Power Sources 159 (2) (2006) 1147.
[13] J. Fleig, J. Power Sources 105 (2002) 228.
[14] C.C. Chin, R.J. Lin, V.C. Yu, C.W. Wang, E.K. Lin, W.C. Tsai, T.Y. Tseng, IEEE Trans. Appl. Supercond. 7 (2) (1997) 1403.
[15] D.R. Mullins, S.H. Overbury, D.R. Huntley, Surf. Sci. 409 (1998) 307.
[16] K.D. Pollard, H.A. Jenkins, R.J. Puddephatt, Chem. Mater. 12 (2000) 701.
[17] N. Ozer, Sol. Energy, Mater. Sol. Cells 68 (2001) 391.
[18] Y.P. Fu, C.H. Lin, C.S. Hsu, J. Alloys Compd. 391 (2005) 110–114.
[19] A. Qi Wang, T. Diane Golden, J. Electrochem. Soc. 150 (9) (2003) C616.
[20] B. Elidrissi, M. Addon, M. Regraghi, C. Mong, A. Bougrine, A. Kachouane, Thin Solid Films 379 (2000) 23.
[21] M.F. Garcia-Sanchez, G. Rodriquez-Gattorono, Solid State Ionics 96 (1997) 89.
[22] S. Wang, W. Wang, Q. Lia, M. Zhang, Y. Qian, Solid State Ionics 133 (2000) 211.
[23] K. Konstsntinov, I. Stambolova, P. Peshev, Int. J. Inorg. Mater. 2 (2000) 277.
[24] N.L. Petrova, R.V. Todorovsk, D.S. Todorovsky, Solid State Ionics 177 (2006) 613.
[25] R. Gallage, A. Matsuo, T. Watanabe, N. Matsushita, M. Yoshimura, J. Electroceram. 22 (2009) 33.
[26] J.L.M. Rupp, T. Drobek, A. Rossi, L.J. Gauckler, Chem. Mater. 19 (2007) 1134.
[27] B.B. Patil, S.H. Pawar, Appl. Surf. Sci. 253 (2007) 4994.
[28] M.D. Uplane, S.H. Pawar, Solid State Commun. 46 (12) (1983) 847.
[29] K.L. Chopra, Thin Film Phenomena, McGraw Hill Book Co., New York, 1969.
[30] D. Perednis, O. Wilhelm, S.E. Pratsinis, L.J. Gauckler, Thin Solid Films 474 (2005) 84.
[31] CeO_2 Pdf # (cubic): 00-034-0394.
[32] C.O. Avellaueda, M.A.C. Beratan, M. Regragui, C. Monty, A. Bougrine, A. Kachouane, Thin Solid Films 379 (2000) 23.
[33] M. Wolcyrz, L. Kepinski, J. Solid State Chem. 99 (1992) 409.
[34] B.B. Patil, V. Ganesan, S.H. Pawar, J. Alloys Compd. 460 (2008) 680.
[35] Y. Zhou, M.N. Rahaman, Acta Mater. 45 (1997) 3635.
[36] I. Zhitomirsky, A. Petric, Mater. Lett. 40 (1999) 263.
[37] S. Bertaux, P. Reynders, Jean-Marc Heintz, Thin Solid Films 473 (2005) 80.

[38] M. Krunks, E. Mellikov, Thin Solid Films 270 (1995) 33.
[39] B. Elidrissi, M. Addon, M. Regraghi, C. Mong, A. Bougrine, A Kachouane, Thin Solid Films 379 (2000) 23.
[40] R. Kassing, W. Bax, Jpn. J. Appl. Phys. (Suppl. 2 Pt. 1) (1974) 801.
[41] H. Yahira, Y. Egushi, K. Eguschi, H. Aria, J. Appl. Electrochem. 18 (1998) 527.
[42] G.B. Jung, T.J. Haung, C.L. Chang, J. Soild State Electrochem. 6 (2002) 225.
[43] C. Peng, Y. Zhang, Z.W. Cheng, X. Cheng, J. Meng, J. Mater. Sci.: Mater. Electron. 13 (2002) 757.
[44] Hooper, J. Appl. Phys. 10 (1976) 1487.
[45] S. Sameshima, H. Ono, K. Higashi, K. Sonoda, P. Hirata, Y. Ikuma, J. Ceram. Soc. Jpn. 108 (12) (2000) 1058.
[46] T.S. Zhang, J. Ma, S.H. Chan, P. Hing, J.A. Kilner, Solid State Sci. 6 (2004) 565.
[47] Piotr Jasinski, Solid State Ionics 177 (2006) 2509.
[48] Piotr Jasinski, Vladimir Petrovsky, Toshio Suzuki, Harlan U. Anderson, J. Electrochem. Soc. 152 (4) (2005) J27.
[49] C. Peng, Y. Zhang, Z.W. Cheng, X. Cheng, J. Meng, J.Mater. Sci.: Mater. Electron. 13 (2002) 757.
[50] J.L.M. Rupp, A. Infortuna, L.J. Gauckler, J. Am. Ceramic Soc. 90 (6) (2007) 1792.
[51] H.L. Tuller, Solid State Ionics 131 (2000) 143.
[52] R. Gerhardt, A.S. Nowick, J. Am. Ceram. Soc. 69 (1986) 641.
[53] Y.M. Chiang, E.B. Lavik, I. Kosacki, H.L. Tuller, J.Y. Ying, Appl. Phys. Lett. 69 (1996) 186.